Supporting Information

Structure Transformation of a Luminescent Pillared-Layer Metal−Organic Framework Caused by Point Defects Accumulation

Yi Qi, Huoshu Xu, Xiaomin Li, Binbin Tu, Qingqing Pang, Xiao Lin, Erlong Ning, Qiaowei Li*

Department of Chemistry, iChEM (Collaborative Innovation Center of Chemistry for Energy Materials), and Shanghai Key Laboratory of Molecular Catalysis and Innovative Materials, Fudan University, Shanghai 200433, P. R. China

*Email: qwli@fudan.edu.cn

1. Materials synthesis

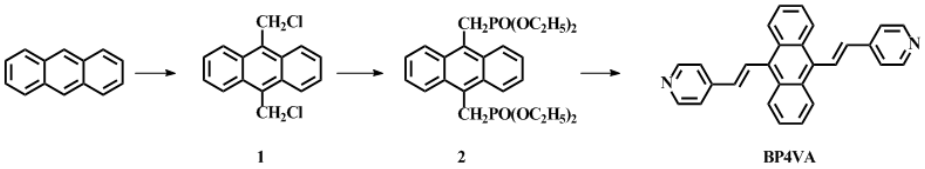

Scheme S1. Synthetic Pathway to 9,10-bis((E)-2-(pyridin-4-yl)vinyl)anthracene (BP4VA)[1].

Synthesis of 9,10-bis(chloromethyl)anthracene (1). Anthracene (18.0 g, 0.1 mol) was dissolved into a mixed solution of 1,4-dioxane (144 mL) and concentrated HCl (30 mL) in an oven-dried round bottle flask. Paraformaldehyde (15.2 g) was added to the solution and the mixture was stirred for 2 h at 110 °C under reflux with ice cold water in the condenser. The reaction was kept under stirring for 4 h after heating was stopped. The reaction mixture was then washed by 1,4-dioxane and H_2O to give compound **1** as yellow powder 12.3 g (40% yield). ^{1}H NMR (400 MHz, DMSO-d_6) δ 8.53 (s, 4H), 7.67 (s, 4H), 5.87 (s, 4H). ^{13}C NMR (101 MHz, DMSO-d_6) δ 131.14 (s), 129.69 (s), 127.22 (s), 125.19 (s). High resolution MS (HRMS), Calcd. for $C_{16}H_{12}Cl_2$: m/z 275.0394, Found: 275.0399.

Synthesis of tetraethyl(anthracene-9,10-diylbis(methylene))bis(phosphonate) (2). 1 (3.4 g, 10 mmol) was dissolved in $P(OC_2H_5)_3$ (18 mL, 0.1 mol). The reaction mixture was heated in an oil bath to 150 °C and stirred for 18 h under N_2 atmosphere. After being cooled to room temperature, the reaction mixture was poured into petroleum ether and filtered to give 3.5 g of **2** as a light yellow solid (70% yield). ^{1}H NMR (400 MHz, $CDCl_3$) δ 8.37 (s, 4H), 7.54 (s, 4H), 4.17–4.27 (s, 4H), 3.94–3.73 (m, 8H). ^{13}C NMR (101 MHz, $CDCl_3$) δ 130.30 (s), 125.64 (d, J = 19.8 Hz), 124.39–124.09 (m), 62.15 (t, J = 3.4 Hz), 28.08 (d, J = 3.9 Hz), 26.66 (d, J = 4.0 Hz), 16.24 (t, J = 3.0 Hz) HRMS, Calcd. for $C_{24}H_{32}O_6P_2$: m/z 479.1752, Found: 479.1747.

Synthesis of BP4VA. 2 (0.500 g, 1.04 mmol) was added into a solution of 2 M *n*-BuLi (2 mL, 4 mmol) in THF (70 mL) and stirred under nitrogen in an ice-bath. After adding a solution of picolinaldehyde (0.25 mL, 2.53 mmol) in THF (70 mL), the mixture was stirred overnight at room temperature. The resultant precipitate was washed with MeOH and filtered off to give yellow BP4VA powder (40% yield). ^{1}H NMR (400 MHz, $CDCl_3$) δ 8.70 (dd, J = 4.6, 1.5 Hz, 4H), 8.33 (dd, J = 6.8, 3.3 Hz, 4H), 8.16 (d, J = 16.4 Hz, 2H), 7.54 (dd, J = 4.8, 1.7 Hz, 4H), 7.53−7.49 (m, 4H), 6.90 (d, J = 16.5 Hz, 2H). ^{13}C NMR (101 MHz, $CDCl_3$) δ 150.49 (s), 144.24 (s), 135.28 (s), 132.08

(s), 129.92 (s), 129.39 (s), 126.15 (s), 125.80 (s), 120.97 (s). HRMS, Calcd. for $C_{28}H_{20}N_2$: m/z 385.1705, Found: 385.1722.

Synthesis of [Zn_2(BPDC)$_2$(BP4VA)] (FDM-22, BPDC = 1,1'-biphenyl-4,4'-dicarboxylic acid). Zinc nitrate hexahydrate $Zn(NO_3)_2 \cdot 6H_2O$ (59.4 mg, 0.2 mmol), BPDC (22.4 mg, 0.1 mmol), and BP4VA (19.2 mg, 0.05 mmol) were dissolved in 15 mL *N,N*-dimethylacetamide (DMA) to form a light yellow clear solution in a 25-mL vial. The vial was capped tightly, placed in a 100 °C oven for 15 h, and then transferred to a 65 °C oven for 24 h. Light yellow block crystals were obtained and rinsed with 25 mL DMA for five times. Yield: 67 % based on BP4VA. Sample for elemental analysis was solvent exchanged by acetone for nine times over three days and followed by heating at 100 °C for 6 hours under dynamic vacuum. Formula: $Zn_2C_{56}H_{36}N_2O_8$, Cal (%): C = 67.55, H = 3.64, N = 2.81, Zn = 13.13. Found (%): C = 65.46, H = 3.94, N = 2.67, Zn = 13.21. FT-IR: (KBr 450−4000 cm^{-1}): 3420 (s), 1637 (s), 1608 (vs), 1541 (s), 1389 (vs), 1224 (s), 1174 (s), 1101 (s), 1069 (s), 1028 (s), 1005 (s), 974 (s), 842 (s), 796 (w), 771 (vs), 731 (w), 703 (w), 678 (w), 577 (w), 525 (w), 445 (w).

Preparation of the solvent-removed FDM-22. Prior to the removal of solvent, FDM-22 was solvent exchanged with bench solvent acetone for nine times over three days. Three different methods were used to obtain the dry samples. a) Dry with Supercritical CO_2: acetone was removed with supercritical liquid CO_2 in a Tousimis Samdri PVT-3D critical point dryer by the following procedures. The wet sample was placed inside the dryer and the acetone was exchanged with CO_2(L) over a period of 20 minutes, during which time the liquid CO_2 was vented under positive pressure. The rate of venting of CO_2(L) was kept below the rate of filling so as to maintain a full chamber. After 20 minutes of venting and soaking with CO_2(L), the temperature was raised to 40 °C. The chamber was held above the critical point, with the pressure around 1300 psi, for 1 hour at which point the chamber was slowly vented over the course of 12 hours. b) Dry in the Air: after the solvent was decanted from the vial, crystals were directly exposed to the air in an uncapped 20-ml vial for 24 hours (designated as **FDM-22A**). The phase transformation happens within the first 10 mins, as checked by PXRD (see Figures S3 and S4). The structure remains unchanged for 24 hours, and we think the degradation of the structure due to hydrolysis is insignificant during this period. c) Dry under dynamic Vacuum at elevated temperature: the acetone exchanged FDM-22 was dried under dynamic vacuum at 115 °C for 6 h (designated as **FDM-22V**).

2. Single crystal structure determination

Single crystal of FDM-22 sealed in a 0.3 mm diameter capillary was mounted on a Bruker SMART Apex II single-crystal X-ray diffractometer equipped with a CCD area detector at 258 K. The operating voltage and current were 50 kV, 30 mA to generate Mo *Kα* radiation (λ = 0.71073 Å). The crystal structure was solved by Direct Methods and refined on F^2 by full-matrix least-squares using the Shelxtl-2014[2] software package. The details of crystal information are listed in Table S1. CCDC 1822324 contains the crystallographic data for this file. This data can be obtained free of charge from the Cambridge Crystallographic Data Centre via http://www.ccdc.cam.ac.uk/Community/Requestastructure/pages/Requestastructure.aspx.

In the Checkcif report, the three unsolved Alert level As that were described as 'The value of R_{int} is greater than 0.25', 'The value of R_{int} is greater than 0.12', and 'The value of sine(theta_max)/wavelength is less than 0.550'. These alerts were ascribed to poor single crystal quality. Diffraction spots from multiple domains in the single piece of crystal overlap severely, and could not be separated by data processing software. These diffractions have caused elevated R_{int} value. We found that the perfect crystals without any cracks under optical microscope were proved to be crystals with multi-domains by single-crystal X-ray diffraction, and this problem presented in more than 30 crystals we picked. Analyzed using the 'cell_now' program, diffractions from most of these crystals can be divided into more than 3 different domains. Even if crystals with larger size were selected, better data could not be obtained in more than 10 diffraction collections.

Despite of limited data improvement and high R_{int} (0.3274 and 0.3005 before and after SQUEEZE[3] is applied, respectively) due to multiple crystal domains, we managed to solve the structure based on complete data. As listed in the *cif* file, constrains were used to stabilize the whole structure. ISOR constrains were used for atom C1, C6, C7, C10, C13, C14, C16, C19, and N1. SIMU and DELU constrains were applied for N1, C8, C9, C10, and C11.

We presume the solvent in the pores is DMA, because the only solvent used in the reaction is DMA (and trace amount of water from the metal salt hydrate). (1) Based on the void volume in each U.C. (3282 $Å^3$) and residual electron counts (947 per U.C.) calculated from SQUEEZE, the solvent is 4.9 DMA per [Zn(BPDC)$(BP4VA)_{1/2}$] formula; (2) Based on the void volume in each U.C. (3282 $Å^3$) and an estimation of DMA molecule size (154 $Å^3$, calculated from the DMA solvent density

0.94 g cm^{-3}), the solvent is 5.3 DMA per formula.

Table S1. Single-crystal data of FDM-22.

Structure	FDM-22
Empirical formula based on atoms located by single X-ray diffraction	$ZnC_{28}H_{18}NO_4$
Formula weight	497.80
Temperature	258(2) K
Wavelength	0.71073 Å
Crystal system	Monoclinic
Space group	*C*2/*m*
Unit cell dimensions	a = 22.03(4) Å b = 21.02(3) Å c = 15.27(3) Å β = 131.61(3)°
Volume	5287(16) $Å^3$
Z	4
Density (calculated)	0.625 Mg/m^3
Absorption coefficient	0.480 mm^{-1}
F(000)	1020
Crystal size	0.32 × 0.21 × 0.13 mm^3
Theta range for data collection	1.649 to 20.290°
Index ranges	-20<=h<=21 -20<=k<=20 -14<=l<=10
Reflections collected	8490
Independent reflections	2557 [R(int) = 0.3005]
Completeness	95.9%
Absorption correction	none
Refinement method	Full-matrix least-squares on F^2
Data / restraints / parameters	2557/85/196
Goodness-of-fit on F^2	1.003
Final R indices [I>2sigma(I)]	R1 = 0.1419, wR2 = 0.3596
R indices (all data)	R1 = 0.1661, wR2 = 0.3777
Largest diff. peak and hole	1.579 and -0.928 e$Å^3$

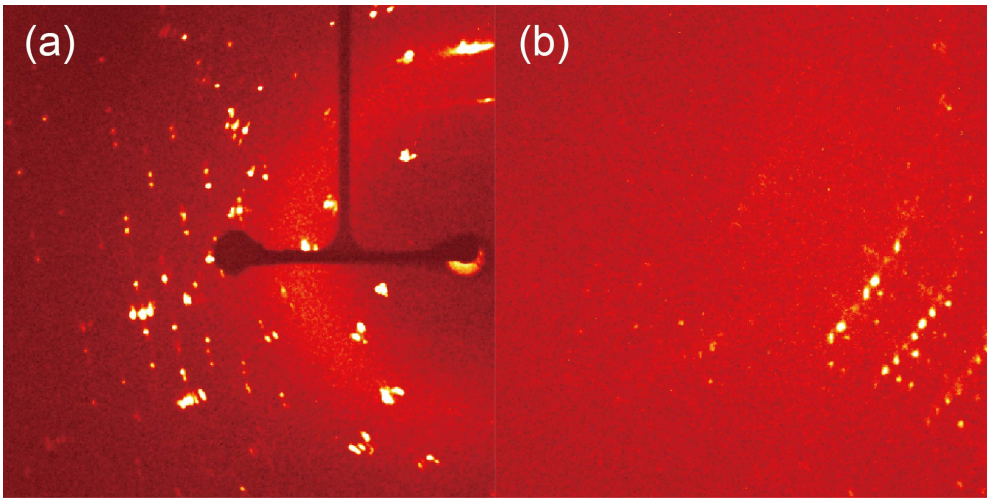

Figure S1. Examples of single crystal X-ray diffraction patterns of FDM-22.

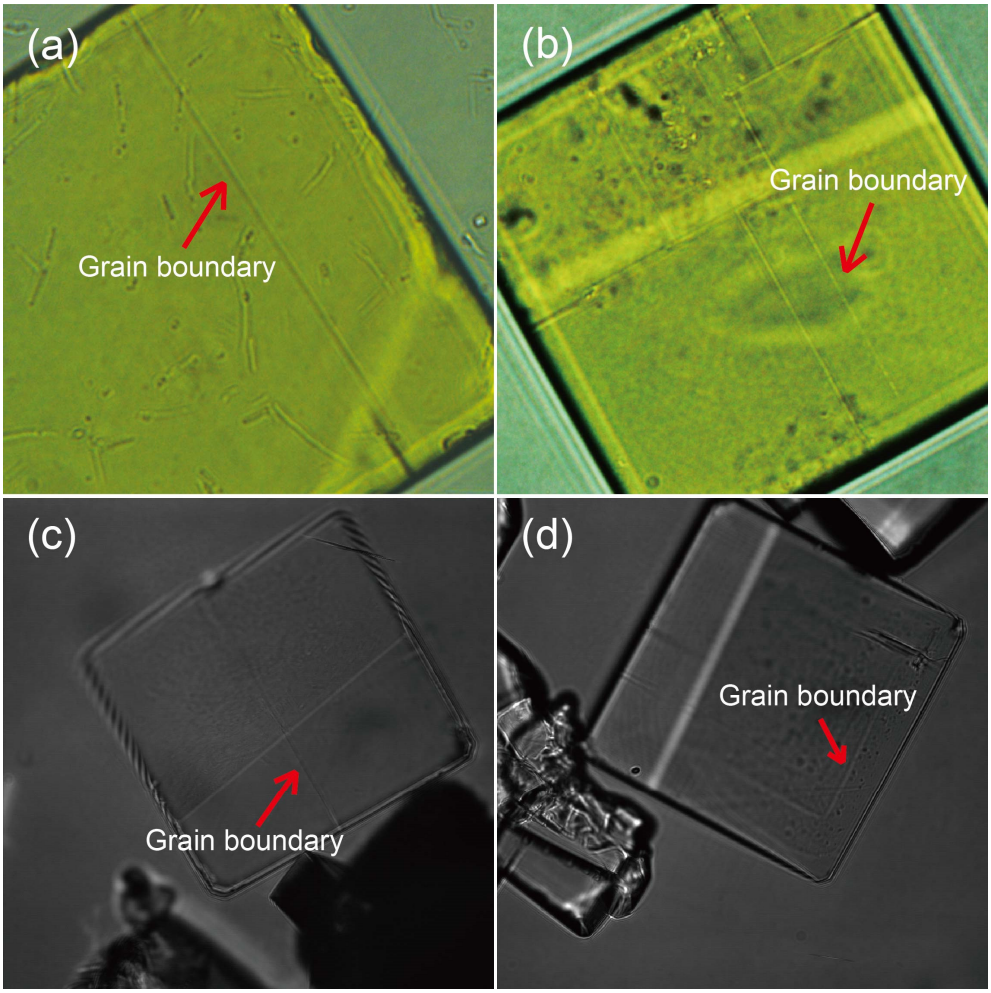

Figure S2. High-resolution optical images of the FDM-22 crystals under optical microscope.

3. Powder X-ray diffraction (PXRD) analysis

The powder X-ray diffraction analysis was performed on a Bruker AXS D8 Advance diffractometer operating at 1600 W power (40 kV, 40 mA) using Cu *Kα* radiation. Simulated PXRD pattern was calculated by the corresponding single crystal structure using Mercury 3.8.

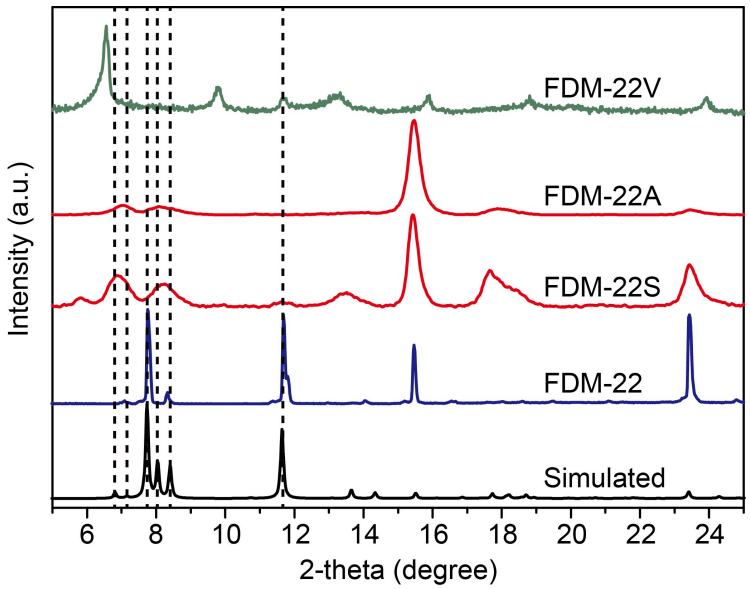

Figure S3. The PXRD patterns of FDM-22, FDM-22S, FDM-22A, and FDM-22V, along with the simulated pattern based on the single crystal structure of FDM-22 at the range of 5–25°.

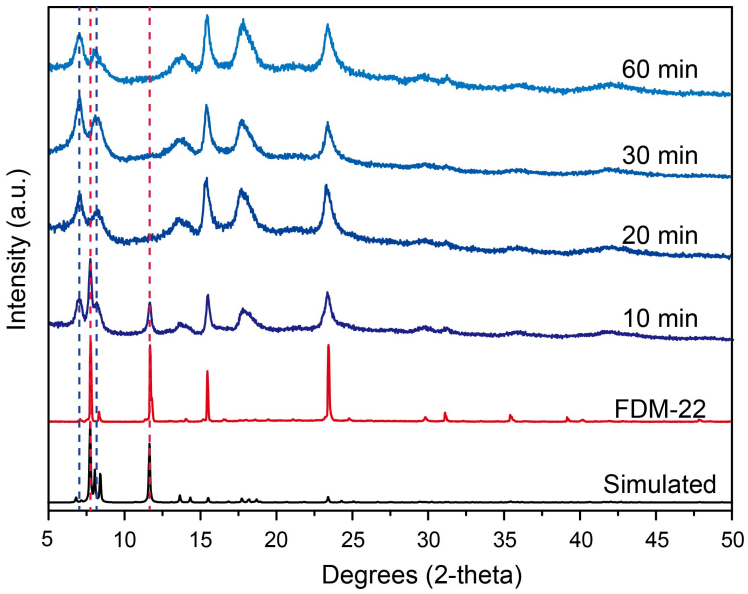

Figure S4. The PXRD patterns of the acetone exchanged FDM-22 after exposed to the air with different duration. Red dashed lines indicate disappeared peaks at 2θ = 7.7° and 11.6°, and blue dashed lines indicate new peaks at 2θ = 7.0° and 8.1°.

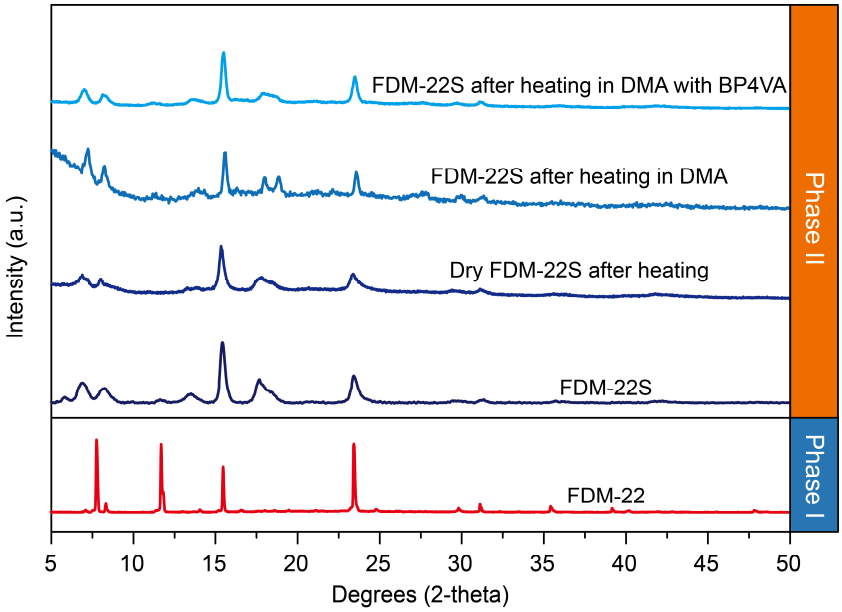

Figure S5. The PXRD patterns of FDM-22, FDM-22S, FDM-22S after 2 d heating without solvent at 100 °C, FDM-22S after 2 d heating in DMA at 100 °C, and FDM-22S after 2 d heating in DMA with the presence of BP4VA at 100 °C.

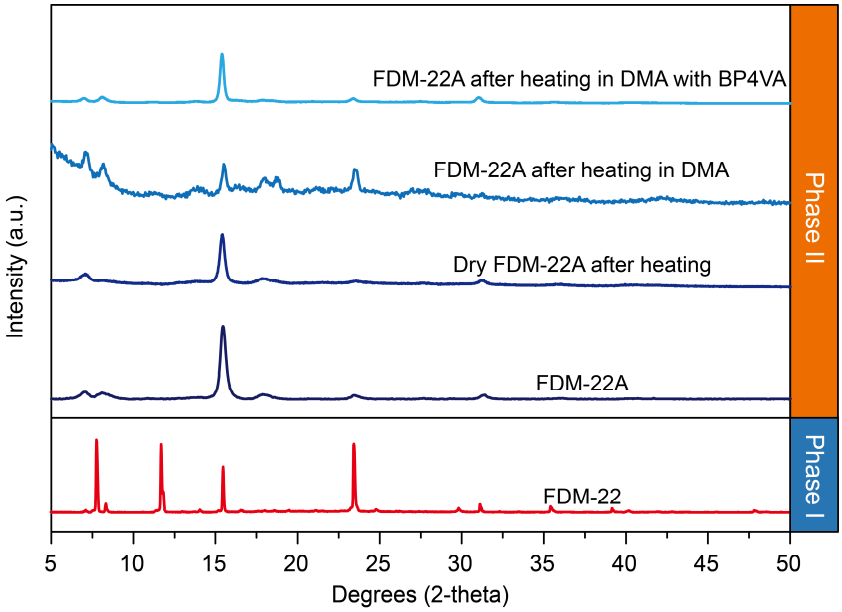

Figure S6. The PXRD patterns of FDM-22, FDM-22A, FDM-22A after 2 d heating without solvent at 100 °C, FDM-22A after 2 d heating in DMA at 100 °C, and FDM-22A after 2 d heating in DMA with the presence of BP4VA at 100 °C.

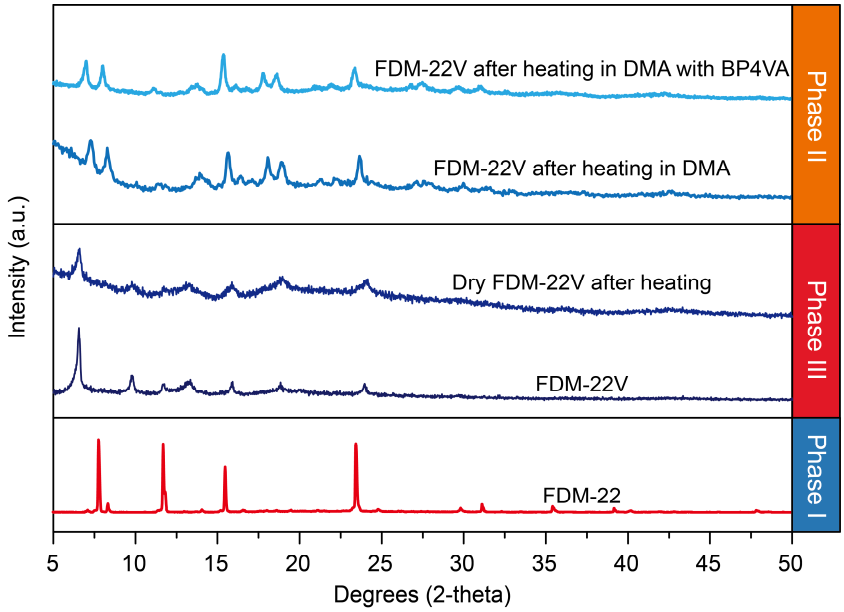

Figure S7. The PXRD patterns of FDM-22, FDM-22V, FDM-22V after 2 d heating without solvent at 100 °C, FDM-22V after 2d heating in DMA at 100 °C, and FDM-22V after 2d heating in DMA with the presence of BP4VA at 100 °C.

4. Crystal images under ambient and UV light

The images were taken with an optical microscope under ambient or UV light. 365 nm UV light was generated by a handhold ultraviolet lamp.

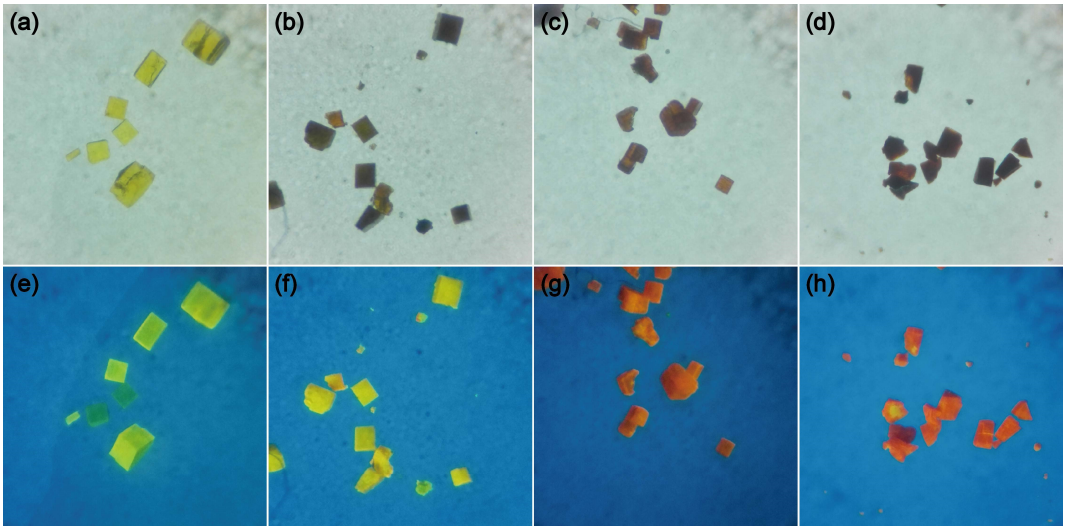

Figure S8. The optical images of FDM-22, FDM-22S, FDM-22A, and FDM-22V under ambient light (a–d) and UV light (e–h), respectively.

5. Luminescence spectroscopy characterization

The luminescence spectra were measured on a Shimadzu RF-5310 Spectrofluorophotometer with a 365 nm activation light for all the samples. For solid state luminescence spectra, the crystals were attached to the quartz slide with transparent tape before positioned in the sample holder. For the luminescence spectra of particles suspended in solvent, the MOF crystals were dispersed in acetone in a cuvette.

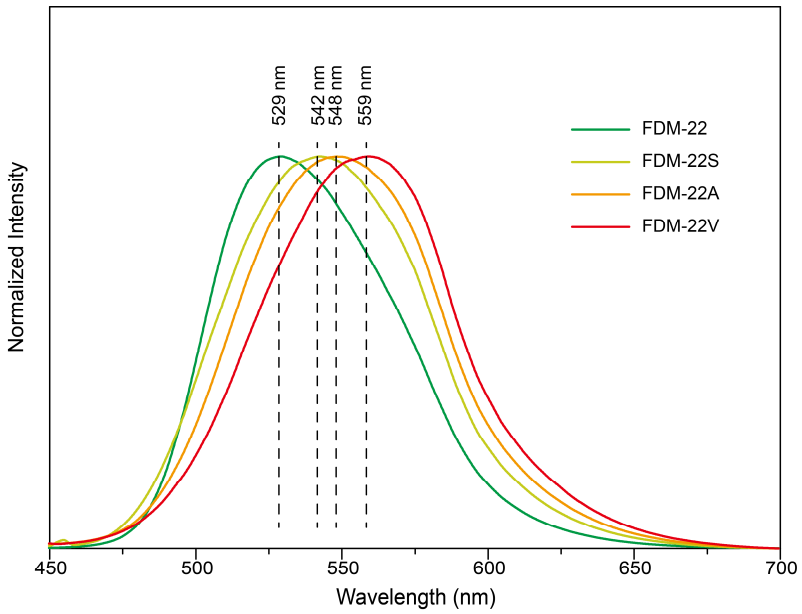

Figure S9. The luminescence spectra of FDM-22, FDM-22S, FDM-22A, and FDM-22V suspended in acetone.

6. MOF morphology by electronic microscopy

The morphology characterization of the MOF was conducted on Phenom ProX scanning electron microscope (SEM) at 15 kV.

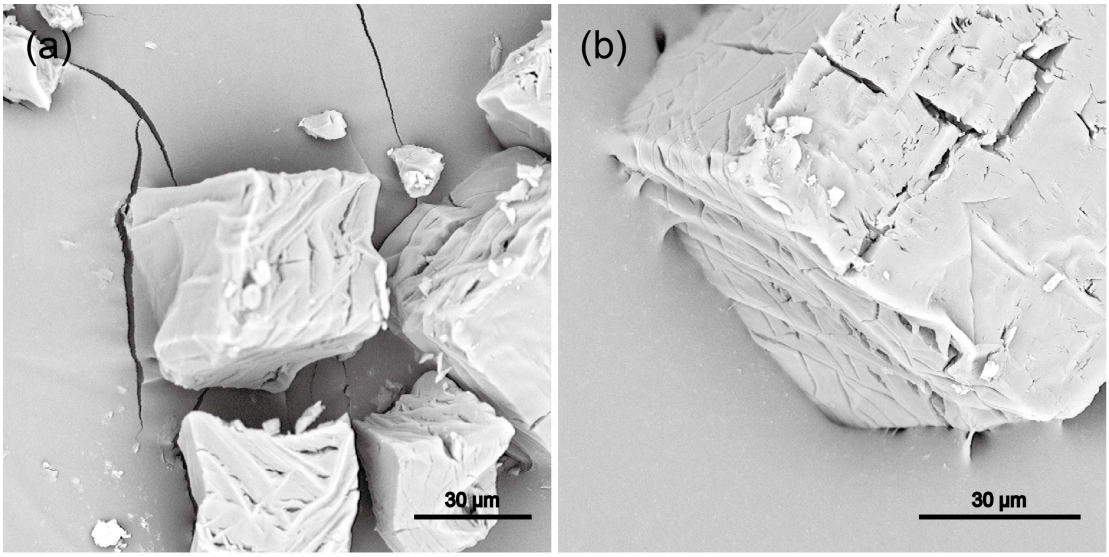

Figure S10. SEM image examples of FDM-22V.

7. N_2 adsorption isotherms

N_2 adsorption measurements were performed on a Quantachrome Autosorb-iQ gas adsorption analyzer at 77 K. Ultra-high purity N_2 was purchased and used as received.

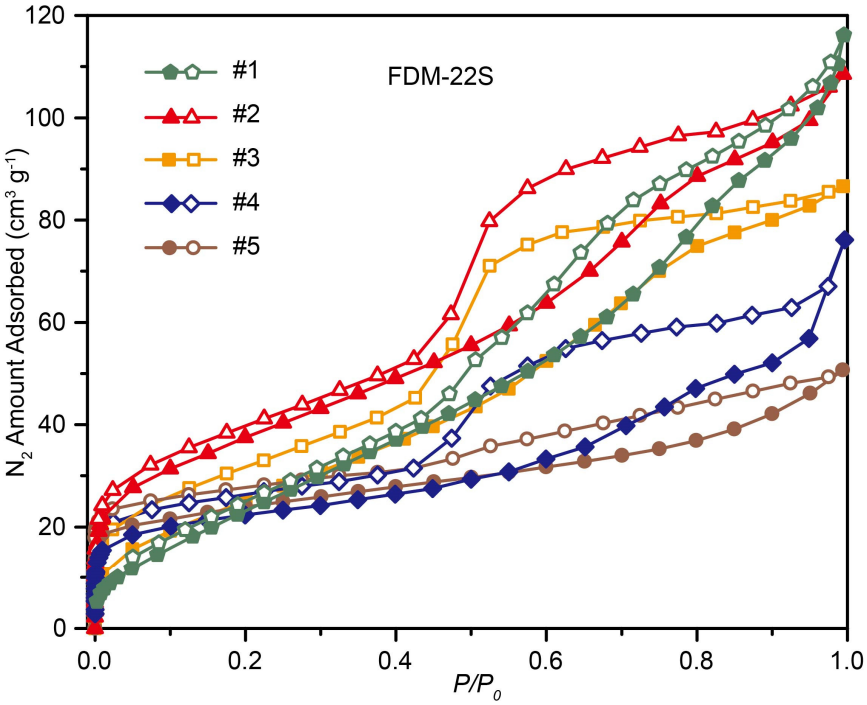

Figure S11. N_2 adsorption isotherms of five parallel FDM-22S samples.

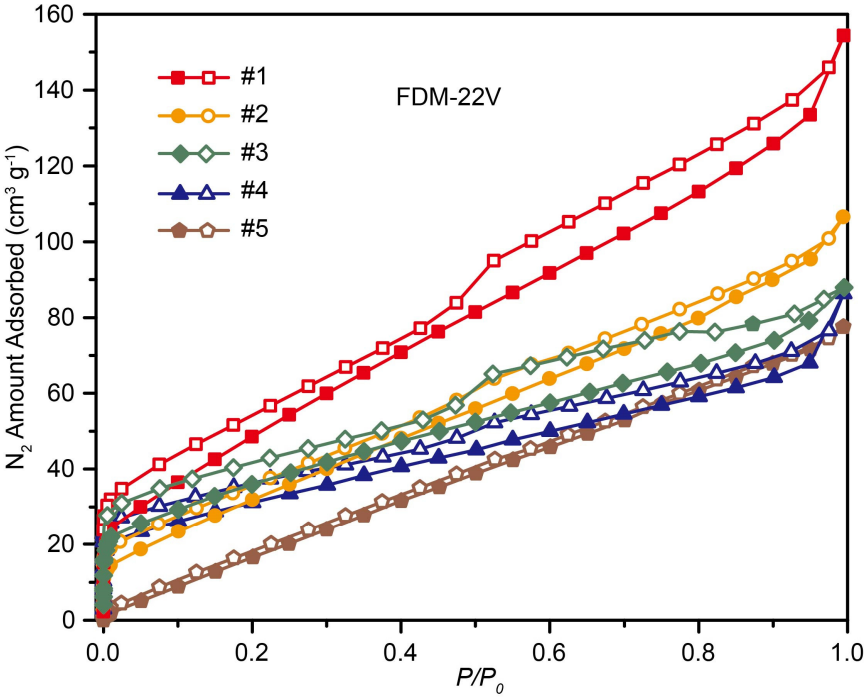

Figure S12. N_2 adsorption isotherms of five parallel FDM-22V samples.

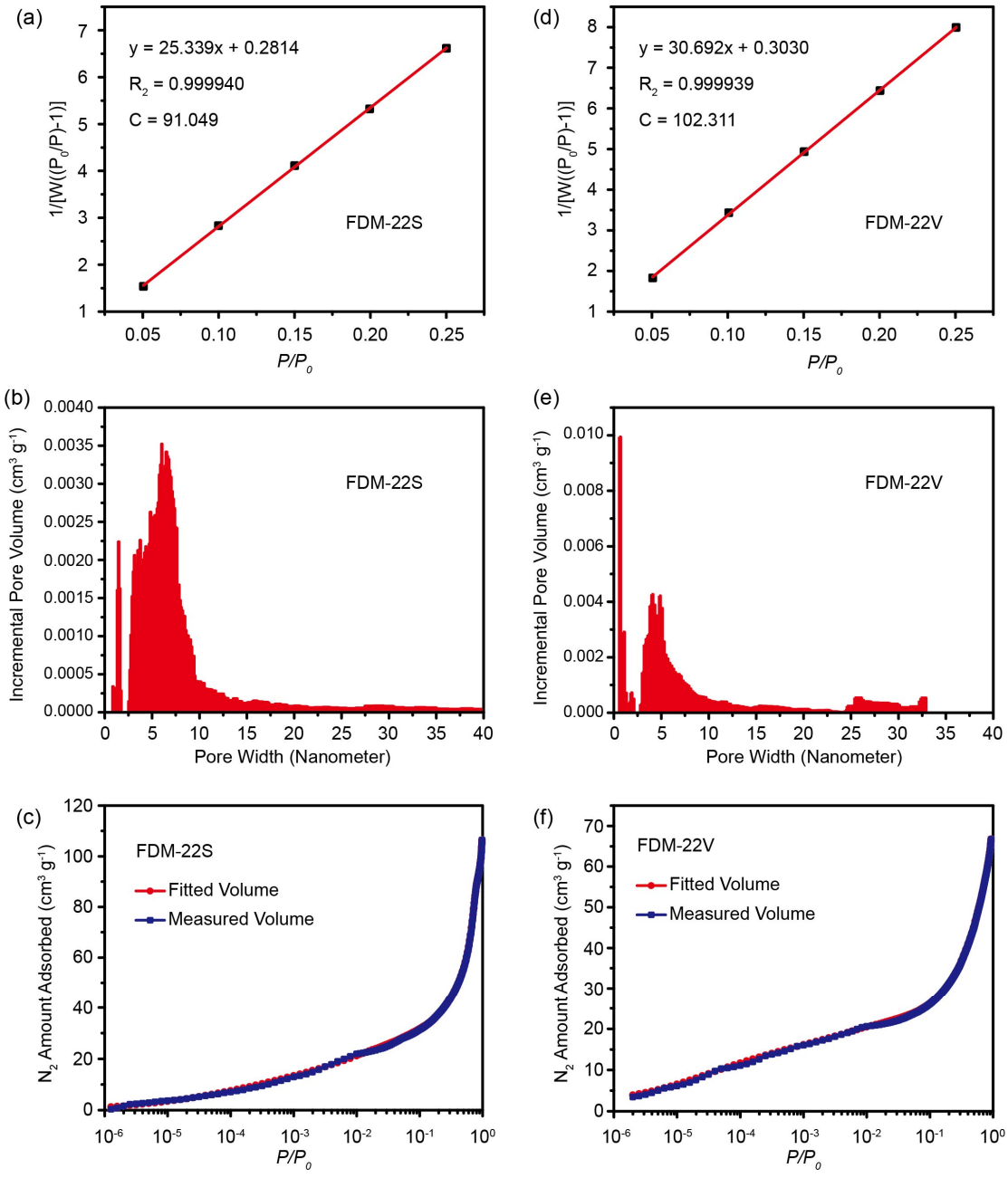

Figure S13. Brunauer–Emmett–Teller (BET) plots of FDM-22S (a) and FDM-22V (d) using the points collected at the pressure range 0.05 to 0.25. Pore size distribution of FDM-22S (b) and FDM-22V (e), in which the pore width corresponds to the diameter of the pore. The adsorption branch NLDFT/ Monte-Carlo fitting comparisons of FDM-22S (c) and FDM-22V (f).

The theoretical surface area of FDM-22 (3201.3 $m^2 g^{-1}$) was calculated based on the accessible surface area per unit cell (1057.8 $Å^2/u.c.$, by Materials Studio 6.1), the density and the cell volume (0.625 g cm^{-3}, 5287 $Å^3$; from crystal structure).

Surface area calculation:

$$\text{Surface Area } (m^2\ g^{-1}) = \frac{\text{Surface Area per Cell } \left(Å^2\right)}{\text{Density } (g\ cm^{-3}) \times \text{Cell Volume } \left(Å^3\right)} \times 10^4$$

8. Raman spectroscopy characterization

The Raman spectra were measured on a HORIBA Jobin Yvon XploRA Raman microscope with a 785-nm laser as excitation source. All spectra were conducted in extended scan mode at the range of 150−2000 cm^{-1}.

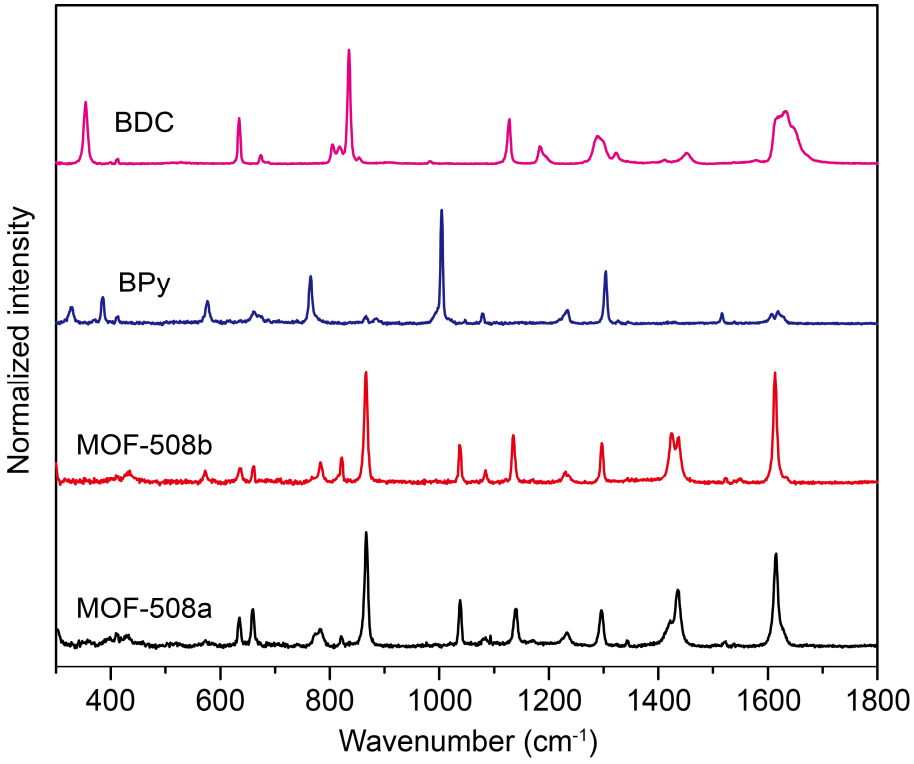

Figure S14. Raman spectra of Benzene-1,4-dicarboxylic acid (BDC), 4,4'-Bipyridine (BPy), MOF-508b (activated form of MOF-508) and MOF-508a (as-synthesized MOF-508)[4].

Table S2. Band assignments of the peaks that correspond to the vibrations of the pyridyl and vinylene groups in BP4VA Raman spectra[5].

Band (cm^{-1})	Assignment
476	Skeletal deformation of C−C=C
969, 991	Breathing vibration of pyridine ring
1203, 1243	C−H in plane bending and stretching vibration in pyridine ring
1312, 1341	C−H in plane bending and stretching vibration in vinylene group
1559	Stretching vibration of pyridine ring
1636	Stretching vibration of C=C double bond

9. X-ray photoelectron spectroscopy (XPS) characterization

The XPS was performed on an ultra-high vacuum PHI5400 system with a non-monochromatic Al X-ray source (Kα = 1486.7 eV) operated at 350 W power. Survey XPS were obtained with analyzer pass energy of 178.5 eV and step size of 1 eV. High resolution spectra were obtained with analyzer pass energy of 35 eV and 0.1 eV energy steps. The binding energy scale was corrected setting C 1s peak at 284.8 eV. The peak fitting was performed with Casa XPS software.

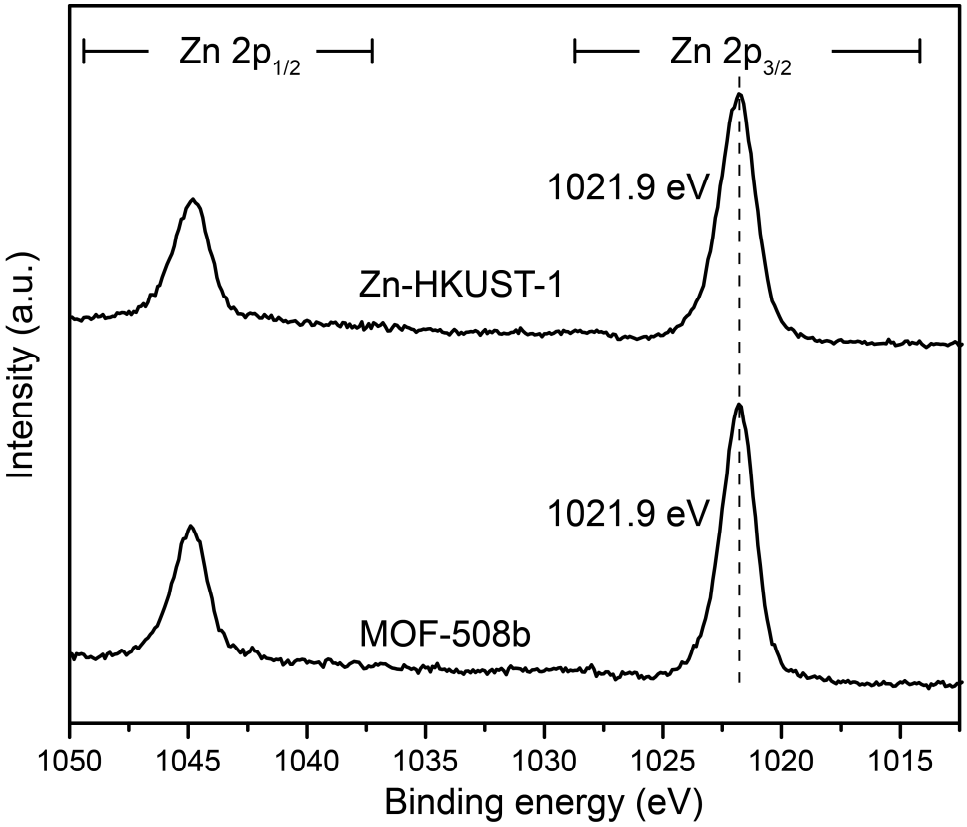

Figure S15. XPS spectra of two model compounds with 5-coordinated Zn(II): MOF-508b (activated form of MOF-508)[4] and Zn-HKUST-1[6].

10. X-ray absorption spectroscopy (XAS) characterization

Zn K-edge XAS were recorded at BL14W1 beamline at Shanghai Synchrotron Radiation Facility (SSRF), Shanghai, China. Storage ring was operated at the energy of 3.5 GeV yielding an electron beam of 130–210 mA. All the powder samples were spread evenly onto a 3M tape and used for the XAS spectra collection in transmission mode using ionization chambers.

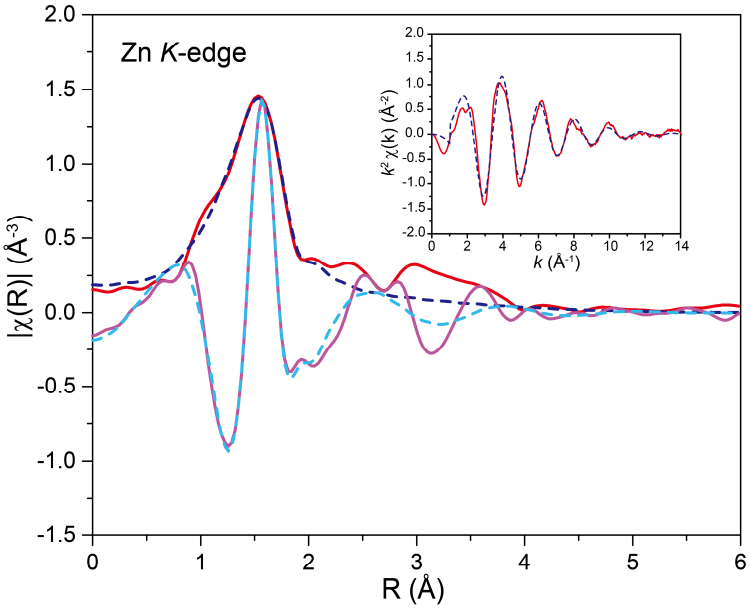

Figure S16. EXAFS fitting results of FDM-22V. Fitting range: 2.44 ⩽ *k* (/Å) ⩽ 13.04 and 1.13 ⩽ *R* (Å) ⩽ 1.93. The inset is k^2-weighted χ(k) data and corresponding fits.

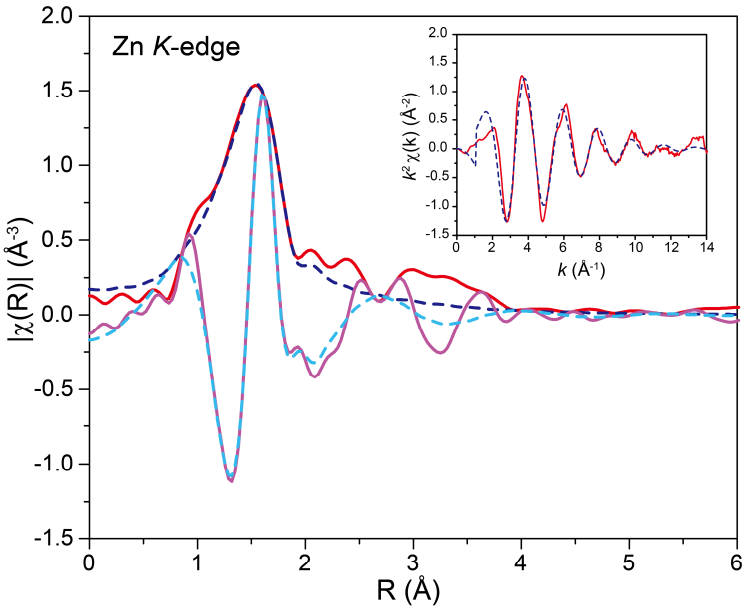

Figure S17. EXAFS fitting results of MOF-508b. Fitting range: 2.34 ⩽ *k* (/Å) ⩽12.83 and 1.13 ⩽ *R* (Å) ⩽ 1.92. The inset is k^2-weighted χ(k) data and corresponding fits.

11. Thermogravimetric (TGA) analysis

Thermogravimetric curve was measured on TA Instruments SDT-Q600 TGA from 25 ℃ to

800 °C at a heating rate of 10 °C min^{-1} under N_2 flow. The guest free sample was preprocessed by acetone exchange for nine times over three days, acetone was further removed by heating at 100 °C for 24 h. The as-synthesized sample was preprocessed by washing with DMA followed by filtering to afford wet samples for TGA analysis.

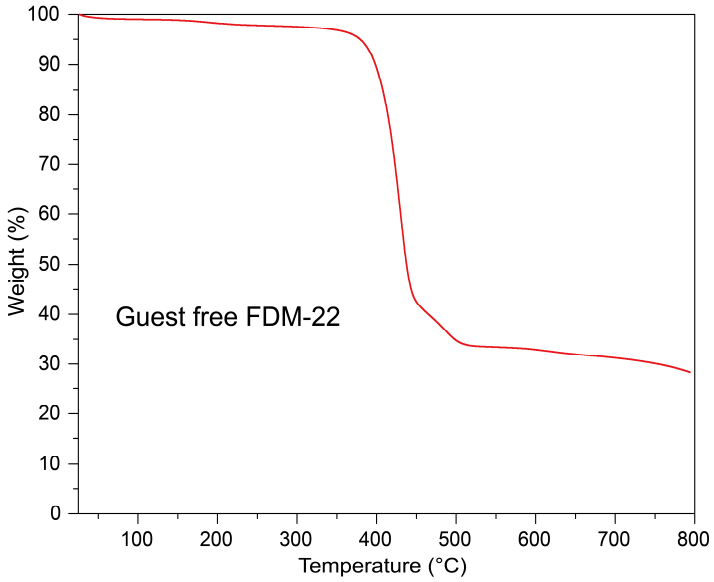

Figure S18. TGA curve of the guest free FDM-22 crystals.

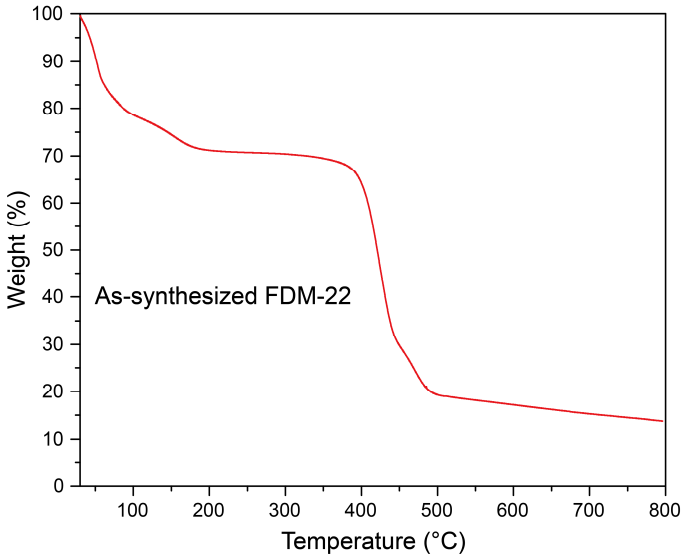

Figure S19. TGA curve of the as-synthesized FDM-22 crystals. Based on the TGA weight loss of the sample before 350 °C, the solvent in the pores is 2.4 DMA per $[Zn(BPDC)(BP4VA)_{1/2}]$ formula. We believe the lower number compared to the solvent content determined by SQUEEZE (see Section 2) is due to the solvent loss during the sample handling.

12. ^{1}H NMR analysis of the digested MOF samples

^{1}H NMR spectra were recorded at 400 MHz with a Mercury plus 400 spectrometer at 298 K. After MOF samples were dissolved in DCl/D_2O and DMSO-d_6, DCl was neutralized by 0.1 M NaOH solution in D_2O to prevent the formation of salt between BP4VA and DCl. The ratio between BPDC and BP4VA in the MOF is calculated by the integration of doublet peak at 8.02 ppm (d, 4H, C-**H^{I}** in BPDC) and the peaks between 7.84 and 7.80 (d, 4H, C-**H^{II}** in BPDC; d, 4H, C-**H^{a}** in BP4VA). For reference, the ratio between BPDC and BP4VA in pristine FDM-22 (with solvent in the pores) was also examined (Figure S20). The ratios of BPDC and BP4VA in FDM-22S, FDM-22A, and FDM-22V are 2:0.91, 2:0.94, and 2:0.92, respectively, which are within error of 10% compared to ideal structure.

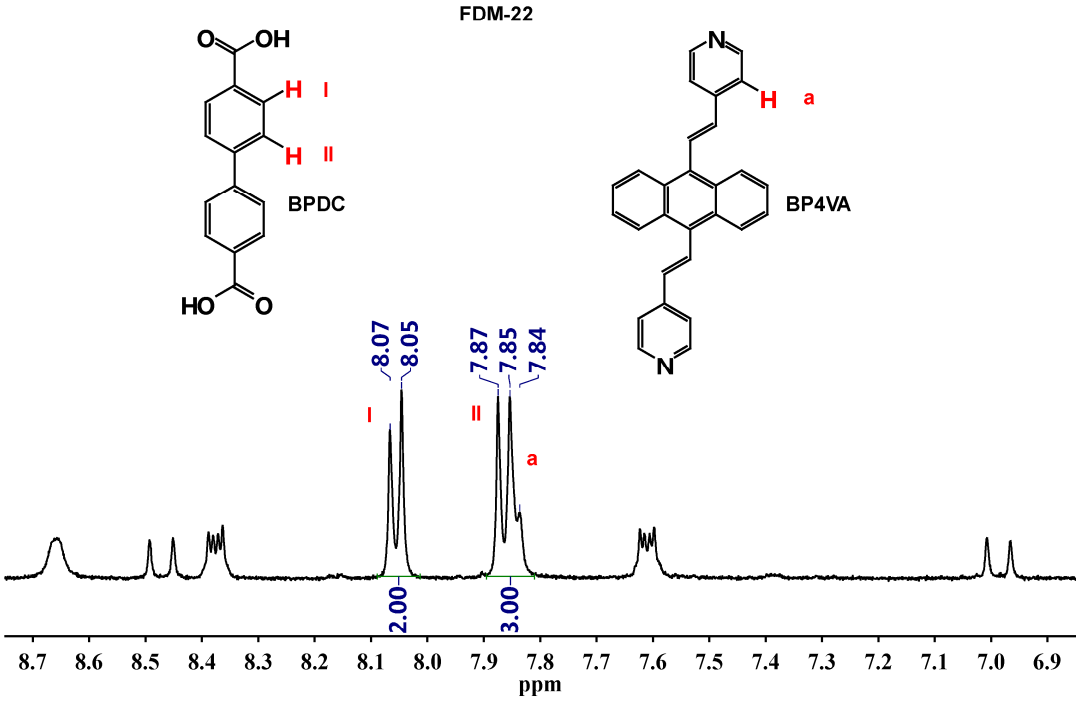

Figure S20. ^{1}H NMR spectrum of the digested FDM-22. Integrations of peaks at 8.06 ppm (d, 4H, C-**H^{I}** in BPDC) and the peaks between 7.87 and 7.84 (d, 4H, C-**H^{II}** in BPDC; d, 4H, C-**H^{a}** in BP4VA) in ^{1}H NMR spectrum show that the ratio of linker BPDC to BP4VA is 2:1.0.

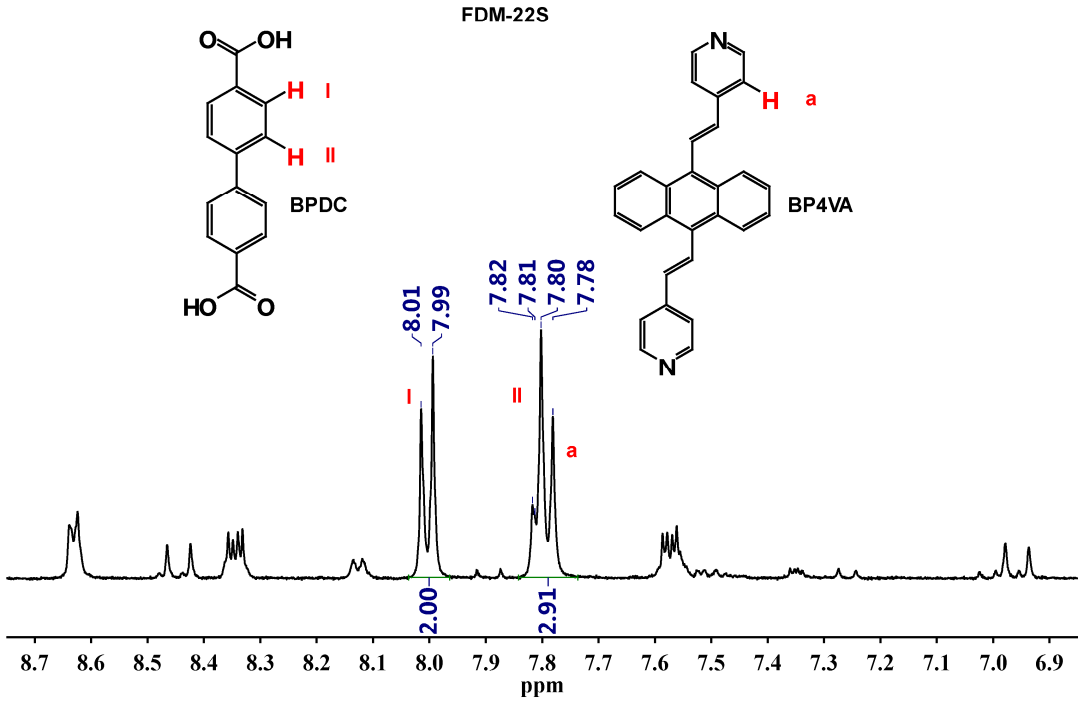

Figure S21. ^{1}H NMR spectrum of the digested FDM-22S. Integrations of peaks at 8.00 ppm (d, 4H, C-**H^{I}** in BPDC) and the peaks between 7.82 and 7.78 (d, 4H, C-**H^{II}** in BPDC; d, 4H, C-**H^{a}** in BP4VA) in ^{1}H NMR spectrum show that the ratio of linker BPDC to BP4VA is 2:0.91.

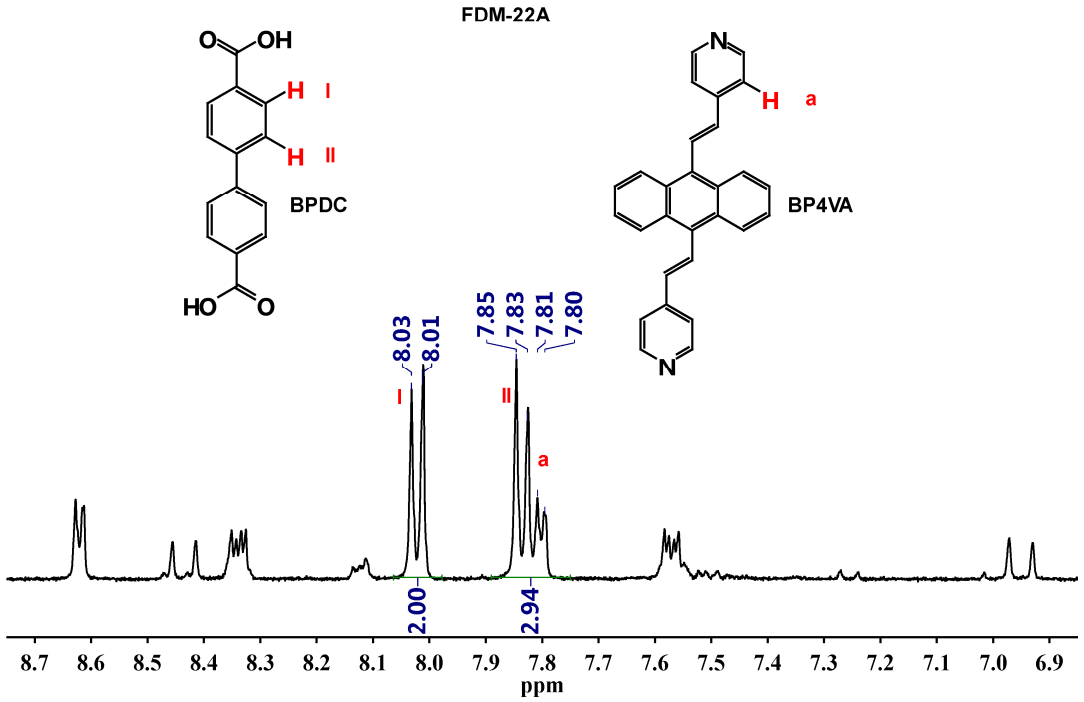

Figure S22. ^{1}H NMR spectrum of the digested FDM-22A. Integrations of peaks at 8.02 ppm (d, 4H, C-**H**$^{\mathbf{I}}$ in BPDC) and the peaks between 7.85 and 7.80 (d, 4H, C-**H**$^{\mathbf{II}}$ in BPDC; d, 4H, C-**H**$^{\mathbf{a}}$ in BP4VA) in ^{1}H NMR spectrum show that the ratio of linker BPDC to BP4VA is 2:0.94.

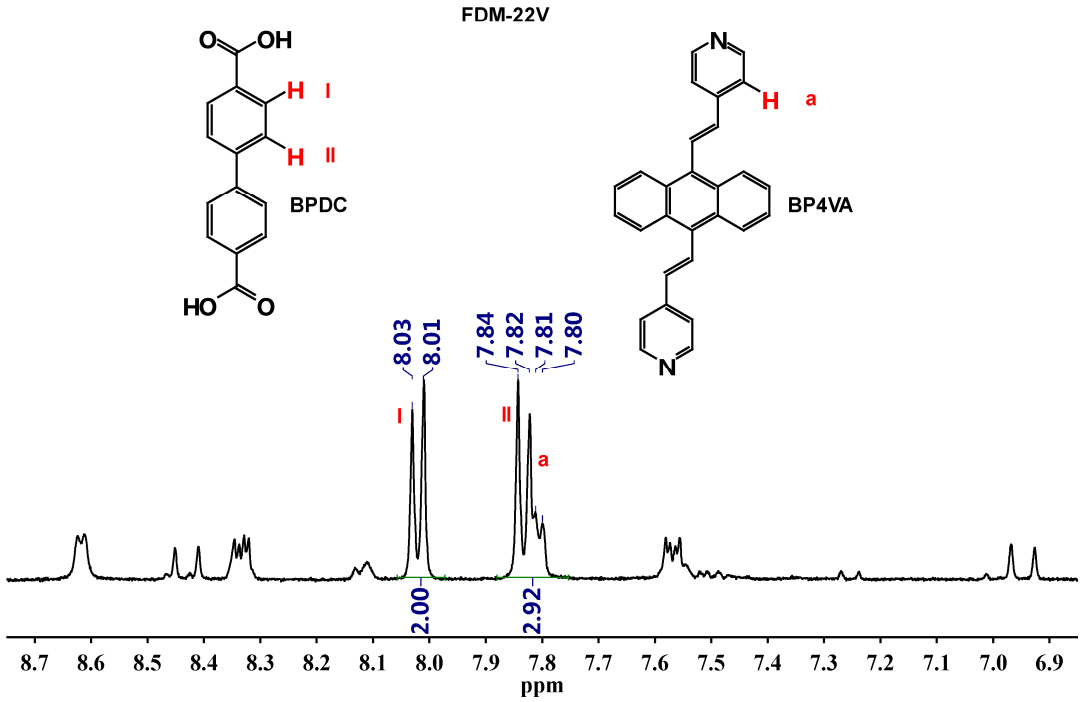

Figure S23. ^{1}H NMR spectrum of the digested FDM-22V. Integrations of peaks at 8.02 ppm (d, 4H, C-**H**$^{\mathbf{I}}$ in BPDC) and the peaks between 7.84 and 7.80 (d, 4H, C-**H**$^{\mathbf{II}}$ in BPDC; d, 4H, C-**H**$^{\mathbf{a}}$ in BP4VA) in ^{1}H NMR spectrum show that the ratio of linker BPDC to BP4VA is 2:0.92.

Reference

(1) Dong, Y.; Zhang, J.; Tan, X.; Wang, L.; Chen, J.; Li, B.; Ye, L.; Xu, B.; Zou, B.; Tian, W. Multi-stimuli responsive fluorescence switching: the reversible piezochromism and protonation effect of a divinylanthracene derivative. *J. Mater. Chem. C* **2013**, 1, 7554-7559.

(2) Sheldrick, G. M. A short history of SHELX. *Acta Crystallogr., Sect. A: Found. Crystallogr.* **2008**, 64, 112-122.

(3) Spek, A. L. Structure validation in chemical crystallography. *Acta Crystallogr., Sect. D: Biol. Crystallogr.* **2009**, 65, 148-155.

(4) Chen, B.; Liang, C.; Yang, J.; Contreras, D. S.; Clancy, Y. L.; Lobkovsky, E. B.; Yaghi, O. M.; Dai, S. A Microporous Metal–Organic Framework for Gas-Chromatographic Separation of Alkanes. *Angew. Chem. Int. Ed.* **2006**, 45, 1390-1393.

(5) Characteristic Raman Frequencies of Organic Compounds; Dollish, F. R., Fateley, W. G., Bentley, F. F., Eds.; Wiley-Interscience: New York, 1974.

(6) Feldblyum, J. I.; Liu, M.; Gidley, D. W.; Matzger, A. J. Reconciling the Discrepancies between Crystallographic Porosity and Guest Access As Exemplified by Zn-HKUST-1. *J. Am. Chem. Soc.* **2011**, 133, 18257-18263.